ISSN 1067-8212, Russian Journal of Non-Ferrous Metals, 2016, Vol. 57, No. 4, pp. 381–388. © Allerton Press, Inc., 2016.

POWDER METALLURGY
OF NONFERROUS METALS AND ALLOYS

Corrosion Resistance and Adhesion of Poly(L-lactic acid)/MgF_2 Composite Coating on AZ31 Magnesium Alloy for Biomedical Application[1]

Zhenlin Wang[a, *] and Ye Guo[a, b, **]

[a] *College of Materials Science and Engineering, Chongqing University of Technology, Chongqing 400054, China*
[b] *Technology Department, Chongqing Changan Automobile Co., Ltd. Chongqing 400023, China*
**e-mail: wzl@cqut.edu.cn;*
***e-mail: wyaow515@tom.com*

Received October 19, 2015

Abstract—Fluoride conversion layer was produced on AZ31 magnesium alloy by soaking in hydrofluoric acid solution and poly(L-lactic acid) (PLLA) film was prepared by spin-coating the PLLA solution. The as-prepared samples were comparatively characterized in phase structure, elements profile, morphology, adhesion force, and corrosion resistance. The results show that more MgF_2 was formed in the outer layer than at the interface which is likely to be composed of MgF_2 and $Mg(OH)_2$. The MgF_2 layer is of labyrinthine porosity with fine pores interconnected to larger ones, while the spin-coated PLLA film is dense and adhere to the substrate seamlessly. PLLA showed a higher adhesion force between the coating and AZ31 substrate than fluoride layer because of its ductility and higher contact area. PLLA was infused into the porous fluoride conversion layer forming an integrated inorganic/organic composite coating. Infiltration of PLLA into MgF_2 layer sealing pores and flaws contributes to reinforcement of the composite coating in favor of improvement of the interfacial adhesion force as well as corrosion resistance. The composite PLLA/MgF_2 coating outperforms either of the solely applied coatings with respect to anticorrosion and adhesion properties under the same condition.

Keywords: poly(L-lactic acid), MgF_2, composite coating, adhesion force, corrosion resistance
DOI: 10.3103/S1067821216040155

INTRODUCTION

Magnesium alloys have been generally viewed as competitive candidates for substitution of conventional bone implant materials thanks to their perfect mechanical properties, easy biodegradation and biocompatibility. However their inherent rapid corrosion rate in physiological environment places hurdle on their extensive clinical applications because the resultant drastic rise in pH value severely deteriorates cell proliferation, differentiation and viability on the implants surface and even trigger chronic tissue inflammatory reaction and blood clots [1, 2]. In recent years, higher requirements on cytocompatibility of implant materials are put forward in addition to their bioactivity, biodegradation and match of mechanical properties. As such, the emerging prerequisite for the extensive biomedical application of magnesium alloy implants increasingly demands minimized corrosion rate, enhanced interfacial adhesion and improved cytocompatibility that facilitates the growth and healing of host tissue.

So far, alloying and surface modification are the two main methods commonly used to improve the corrosion resistance of magnesium alloys. The approach of adding alloying elements like rare earth to host magnesium may inevitablely leave potential toxicity affecting the prothesis' biocompatibility and endangering clinical safety [3]. Surface modification however represents a promising alternative solution to this problem, which is implemented just by encrusting the substrate a bioactive degradable coating with more easiness and cost efficiency compared to other technical routes. Inorganic coating e.g. hydroxyapatite (HA) has popularly been applied to magnesium alloy implants in virtue of its outstanding bioactivity, biodegradation, biocompitability and osteoconduction, nevertheless, owing to its brittleness, HA coating may suffer fracturing and peeling off under load. Biodegradable polymer Poly(lactic acid) (PLA), has been widely used as a biomaterial thanks to its notable merits like high ductility, controllable degradation rate, outstanding biocompatibility and versatility to be composited with inorganic fillers. Homogeneous and smooth PLA coatings can be successfully prepared on

[1] The article is published in the original.

the surface of magnesium substrate, but dynamic degradation tests indicated that there was probably an interaction between the magnesium substrate and the PLA coatings undermining the corrosion resistance [4]. However, increase in the PLA coating thickness was found to increase the degradation resistance, but to resulted in limited adhesion strength [5]. Appropriate coupling agent had to be applied between the coating and substrate to effectively strengthen the adhesion therein [6], whereas the selection of coupling agents and their concomitant biological impacts would instead complicate the problems [7]. On the other hand, the acidic byproducts degraded by PLA will eventually expedite the eroding reactions of magnesium alloy and even induce inflammation reaction due to local excessive acidity, an alkaline counterparts normally a inorganic matter may be required to moderate the acidic environment.

Chemical conversion film containing inorganic constitution has been expected to provide an autologous of cohesive layer that may help the bonding of outer bulk coating with the substrate. Hydrofluoric acid (HF) treated magnesium alloy exhibits improvement on corrosion resistance in favor of cellular applications due to the protective MgF_2 film formed on the substrate having the required biocompatibility [8]. MgF_2 film used as interlayer between the HA coating and magnesium substrate was proved beneficial to the adhesion of HA to some degree, while the thin thickness less than 2 μm and the porous configuration seemingly makes it play only a short-term role [9]. Instead, a composite of fluoride conversion film and polymer coating is more likely to reveal full benefits of the individuals and balance out their drawbacks. During the coating process, liquidus polymer dissolved by organic solvent infiltrates the pores as sealant densifying and bonding the transition layer. Cases of such applications have been embodied by studies on WE42 and AZ31 magnesium alloys modified by composite of micro-arc oxidation/poly-L-lactic acid (MAO/PLLA), indicating a rising adhesive strength at the interface, falling corrosion rate and good cytocompatibility [10, 11]. Nonetheless cases of composite coatings of PLLA/MgF_2 on magnesium alloy for biomedical uses are less retrievable and the understanding of their performances especially the interfacial behaviour still needs further elucidation. This work provides some insights into chemical speciation of fluoride conversion layer as well as the interface adhesion and anticorrosion mechanism of the composite coating with the aim to tentatively shed some light on the inconsistent points in the current studies.

EXPERIMENTAL

Coating Procedure

Prior to coating, the as received AZ31 ingots were cut into rectangular coupons with dimensions 30 mm × 20 mm × 2 mm and were polished with SiC paper up to 1000 grit, washed with distilled water and ultrasonically cleaned in acetone and anhydrous ethanol, respectively.

For the chemical conversion treatment, the samples were immersed in an HF solution with concentration of 40 wt % at room temperature for 48 h. The treated specimens, denoted as 'MgF_2' for the subsequent use, were rinsed with distilled water and dried in blowing air.

PLLA with an average molecular weight of about 400000 was provided by Research Centre of Biomaterials and Engineering, Wuhan University of Technology. The similar coating procedure had been reported in our previous work [12]. Briefly, 1 g PLLA was dissolved in 10 mL dichloromethane (DCM) and magnetically stirred for 30 min followed by 15 min ultrasonic dispersion at room temperature. Then the as-prepared suspension was spin-coated on pretreated magnesium alloy samples for 30 s at a rotating speed of 1500 rpm, the coated surface was immediately dried in blowing air. In order to seek thicker coatings, identical procedure was repeated three times. The obtained coating samples were designated as PLLA1/MgF_2, PLLA3/MgF_2 describing spin-coating PLLA onto HF-treated AZ31 one and three times respectively. Similarly, PLLA coated directly on pristine AZ31 one and three times were given the notations of PLLA1 and PLLA3 respectively.

Characterizations

Phase structure of as prepared samples were characterized by X-ray diffraction (XRD) (D/MAX-IIIA) using CuKα radiation with 2θ scanned from 20° to 70° at rate of 0.05°/s.

Elemental depth profiles of the coatings were depicted by means of JY10000RF glow discharge optical emission spectrometry (GDOES) using a copper anode with a diameter of 4mm, with excitation power set at 30 W, pressure at 650 Pa and voltage at 4.5 V.

Morphologies of the coated magnesium alloy samples were observed by a Zeiss field emission scanning electron microscope (SEM). Prior to measurement, the surface was sputtered with gold.

The interfacial adhesion force between coating and the substrate was evaluated in terms of critical load determined by scratch tests, employing a Nanotest system (Micro Materials, Ltd) equipped with a Rockwell diamond indenter with tip diameter of 25 μm. The indenter scratched on the coating at a rate of 5 μm/s under a normal load ramped at a rate of 50 mN/s, applied after displacement of 50 μm until the total scratch length reached 350 μm. The scratch image was captured using an in-situ optical microscope system in order to locate initial failure of the coating.

Electrochemical measurements were carried out on an EG&G 273A type potentiostat, using Pt as the counter electrode, saturated calomel electrode (SCE)

as reference electrode and simulate body fluid (SBF) as aggressive media. The SBF containing NaCl 8.035 g/L, $NaHCO_3$ 0.355 g/L, KCl 0.225 g/L, $K_2HPO_4 \cdot 3H_2O$ 0.231 g/L, $MgCl_2 \cdot 6H_2O$ 0.311 g/L, $CaCl_2$ 0.292 g/L, Na_2SO_4 0.072 g/L, trishydroxymethylaminomethane 6.063 g/L, hydrochloric buffered at pH 7.4 was prepared and preserved at 37°C [13]. The potential was scanned from −2.2 to 1.0 V versus SCE at a scanning rate of 1 mV/s and the measured area of the samples was 0.785 cm^2. The electrochemical parameters were derived by extrapolating linear fitted Tafel region of the recorded potentiodynamic polarization curves. Also from the electrochemical parameters the polarization resistance (R_p) was calculated according to Eq. (1), where I_{corr} is the corrosion current density, β_a and β_c represent anodic and cathodic Tafel slopes, respectively [14, 15].

$$R_p = \frac{\beta_a \beta_c}{2.3(\beta_a + \beta_c) I_{corr}}. \quad (1)$$

RESULTS AND DISCUSSION

Phase Structure

Figure 1 shows the XRD patterns of bare AZ31 magnesium alloy and those with various coatings. Characteristic lines of α-Mg are identified in the patterns for all the samples, but are relatively weakened for the coated ones due to attenuation by the formed films. Dissimilar to untreated AZ31, the HF-treated AZ31 samples has peaks assigned to sellaite-type MgF_2 (PDS#70-0212) as marked in patterns of sample 'MgF_2' and 'PLLA3/MgF_2'. This confirms the expected formation of MgF_2 conversion layer, the low diffraction intensity of which seemingly signifies its considerable thinness. No new peaks appear in XRD patterns of PLLA coated samples, meaning that PLLA film precipitated onto substrate in an amorphous state via thermally induced phase separation (TIPS) of polymer solution. Moreover, the assumed MgO and $Mg(OH)_2$ are not detected by XRD likely because of their contents below detection limit or location is far away from the outer surface.

Elemental Profile

Elemental depth profiles of MgF_2 coated and PLLA1/MgF_2 composite coated sample are displayed in Fig. 2a,b, respectively. It should be noted that for a given element, its concentration is proportional to the intensity and different element has its own scaling coefficient. In addition to Mg, Al and Zn of AZ31 substrate, adventitious elements F, C, H and O appear in the profile graphics. Herein O and H are suggested to originate from hydrocarbons in the environment, and/or from resultant hydroxides formed on magnesium alloy [8, 16, 17]. The substrate immersed in HF aqueous solution was activated to form chemical conversion layer with F, C, H and O digressively distributed inward, meanwhile the main elements Mg, Al and Zn in substrate distributed conversely as revealed in Fig. 2a. The yielded conversion layer can be estimated to be about 2 μm thick just according to the elements depth profile despite inaccuracy as sputtering rate depends on composition which changes with depth.

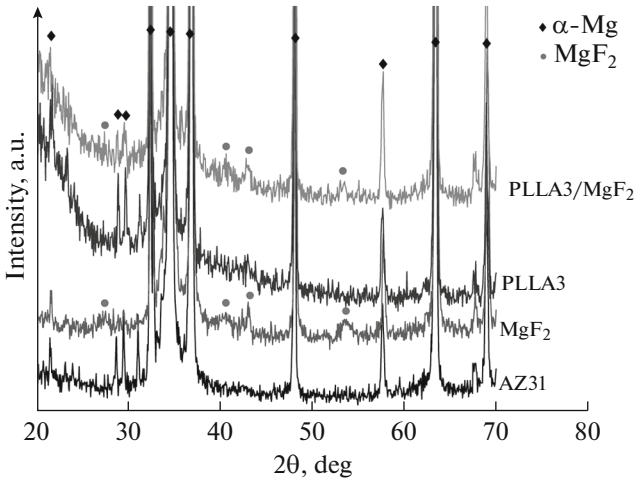

Fig. 1. XRD patterns of the bare and the coated AZ31 magnesium alloy.

It has been generally accepted both MgF_2 and $Mg(OH)_2$ can all be created during HF treatment following the reaction equilibriums below [18]:

$$Mg + 2HF \rightarrow MgF_2 + H_2\uparrow, \quad \Delta_f G^\circ = -477.38\ \text{KJ mol}^{-1}, \quad (2)$$

$$Mg + 2H_2O \rightarrow Mg(OH)_2 + H_2\uparrow, \quad \Delta_f G^\circ = -359.42\ \text{KJ mol}^{-1}, \quad (3)$$

$$Mg(OH)_2 + 2HF \rightarrow MgF_2 + 2H_2O, \quad \Delta_f G^\circ = -117.96\ \text{KJ mol}^{-1}. \quad (4)$$

According to the thermodynamics data, MgF_2 has Gibbs free energy similar to $Mg(OH)_2$, suggesting similar reaction tendency for both processes. However the solubility product constant (K_{sp}) of $Mg(OH)_2$ is 5.61×10^{-12}, an order of magnitude lower than that of MgF_2, $K_{sp} = 5.16 \times 10^{-11}$. In consequence, $Mg(OH)_2$ deposits in preference of MgF_2 forming a barrier to resist further reaction [19]. Further, in presence of HF with high local concentration, a part of the resultant $Mg(OH)_2$ can be converted into MgF_2 precipitates. Alternatively $Mg(OH)_2$ can also be hypothesized to decompose expressed as Eq. (5), but the higher Gibbs free energy may disable the occurrence of this reaction which actually can only take place above 340°C. The

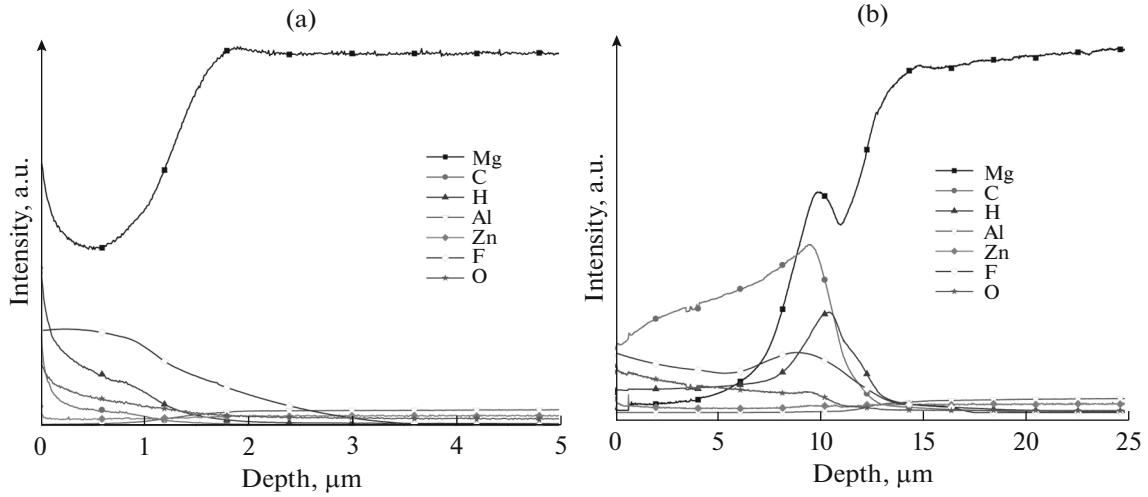

Fig. 2. Elements profile of (a) fluoride treated AZ31 and (b) PLLA/fluoride treated AZ31.

XRD patterns (Fig. 1) rule out the possible presence of MgO yielded by HF soaking.

$$\begin{gathered} Mg(OH)_2 \rightarrow MgO + H_2O, \\ \Delta_f G^\circ = 27.26\ \text{KJ mol}^{-1}. \end{gathered} \quad (5)$$

Given this mechanism, a mixture of MgF_2 and residual $Mg(OH)_2$ close to the substrate appear to bring down Mg concentration because the latter has a lower Mg content than the former. It is proven by the fact that a hump appears on Mg profile close to the substrate matrix, signifying more MgF_2 in the outer layer than in the interface which assumedly composes of MgF_2 and $Mg(OH)_2$.

As shown in Fig. 2b, elemental profiles of PLLA1/MgF_2 indicate newly added PLLA film characterized by additional C and H lines superposing those of the previous MgF_2 layer. The PLLA marked by higher C and H elements is infused into the conversion layer forming a merged zone because C and H profiles have a broad overlapped band with Mg and F within the conversion layer.

Morphology

The cross-sectional morphology of sample MgF_2 (Fig. 3a) shows a uniform fluoride conversion layer adhered to the substrate, but its microstructure is of labyrinthine porosity with fine pores interconnected to larger ones as exhibited in Fig. 3b. The main reason for the formation of the cellular structure of the fluoride film may be the hydrogen evolution during soaking in HF solution [20]. Figure 3c exhibits the side-viewed morphology of PLLA3 coating on AZ31, which reveals about 20 μm of dense PLLA layer adhered uniformly to the substrate. The interface between the polymer and the substrate shown in magnified image (Fig. 3d) is seamless except for few flaws. Dense PLLA film is formed owing to significant volumetric contraction and hence drastic reduction in polymer free volume through TIPS induced by evaporation of DCM and heat dissipation during spin-coating [12].

Composite coating PLLA3/MgF_2 has an extended thickness of about 30 μm with PLLA infiltrated into porous MgF_2 layer leaving visible interpenetrated overlapping edge (Fig. 3e). As demonstrated in the magnified view of the interface (Fig. 3f), the fluoride layer with thickness of about 2 μm is sandwiched firmly between PLLA and the substrate. The fluoride conversion layer is observed impregnated by PLLA forming an integrated inorganic/organic composite coating. This is consistent with the results of PLLA elements distribution into MgF_2, ranging as indicated in Fig. 2b.

Adhesion Force

Figure 4 illustrates the topographic depth (D) as function of scratch displacement (S) of the stylus under ramp-up load (L) applied after 50 μm pre-scan for levelling. The adhesion force between the coating and the substrate is evaluated in terms of critical load (L_c) that represents the onset normal force in the case of a coating failure where the corresponding depth indicates the thickness of the coating (T). In addition, the captured scratch imprint was matched with the recorded curves for precise positioning the failure point. As demonstrated in Fig. 4, values of L_c and T for sample MgF_2, PLLA1, PLLA3, PLLA1/MgF_2 and PLLA3/MgF_2 can be easily read from the corresponding plots and are summarized in Table 1. This methodology provides an effective assessment on critical load most close to the clinical application conditions where implants are mainly subject to compressing or scraping typically in vertical direction.

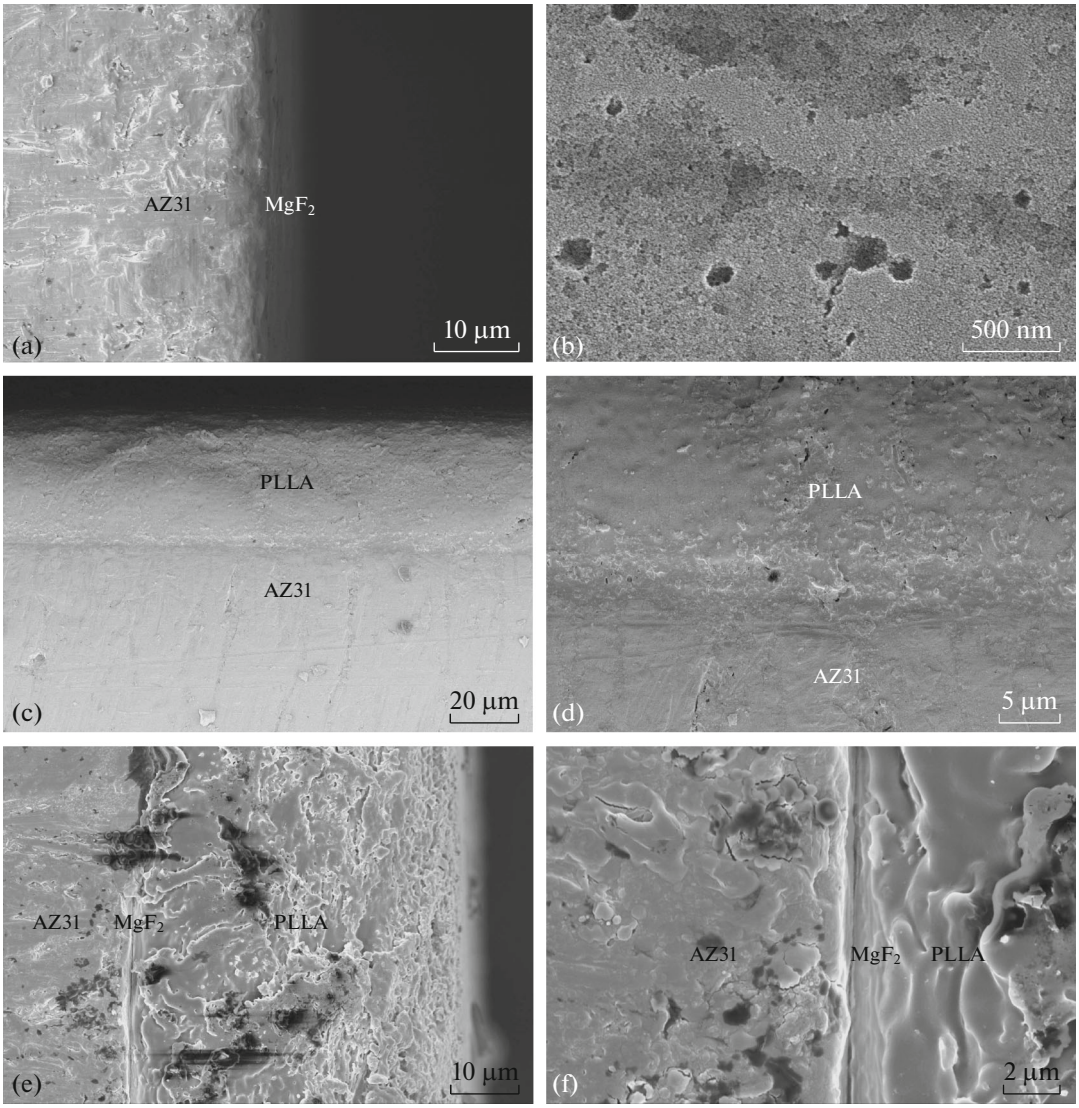

Fig. 3. Morphology of coated AZ31 magnesium alloy: (a) cross sectional image of MgF_2; (b) surface of MgF_2; (c) cross-sectional image of PLLA3; (d) interface of PLLA3; (e) cross-sectional image of PLLA3/MgF_2; (f) interface of PLLA3/MgF_2.

Comparison of the L_c listed in Table 1 indicates that solely coated PLLA film has a higher critical load than MgF_2 layer. Nevertheless, composite coating of PLLA and MgF_2 remarkably improves critical load, and increasing PLLA thickness gives rise to critical load as well. As revealed by the scratch images, the MgF_2 layer cracks abruptly and instead the PLLA-containing coatings are observed to be gradually abraded meaning enhanced wear resistance as compared to the former. Their diverse behaviours are more likely to be associated with brittleness and porosity of MgF_2 layer as compared to ductility and dense microstructure of PLLA. The results are in agreement with the reasonable notion that there is a reaction of carboxyl groups from PLA and hydroxyl radicals from $Mg(OH)_2$ on the surface causing chemical bonding

Table 1. Critical loads and thicknesses of studied coatings on AZ31 magnesium alloy

Sample	MgF_2	PLLA1	PLLA3	PLLA1/MgF_2	PLLA3/MgF_2
L_c (N)	0.480	1.565	1.796	2.067	2.653
T (μm)	1.88	14.94	19.72	15.89	28.36

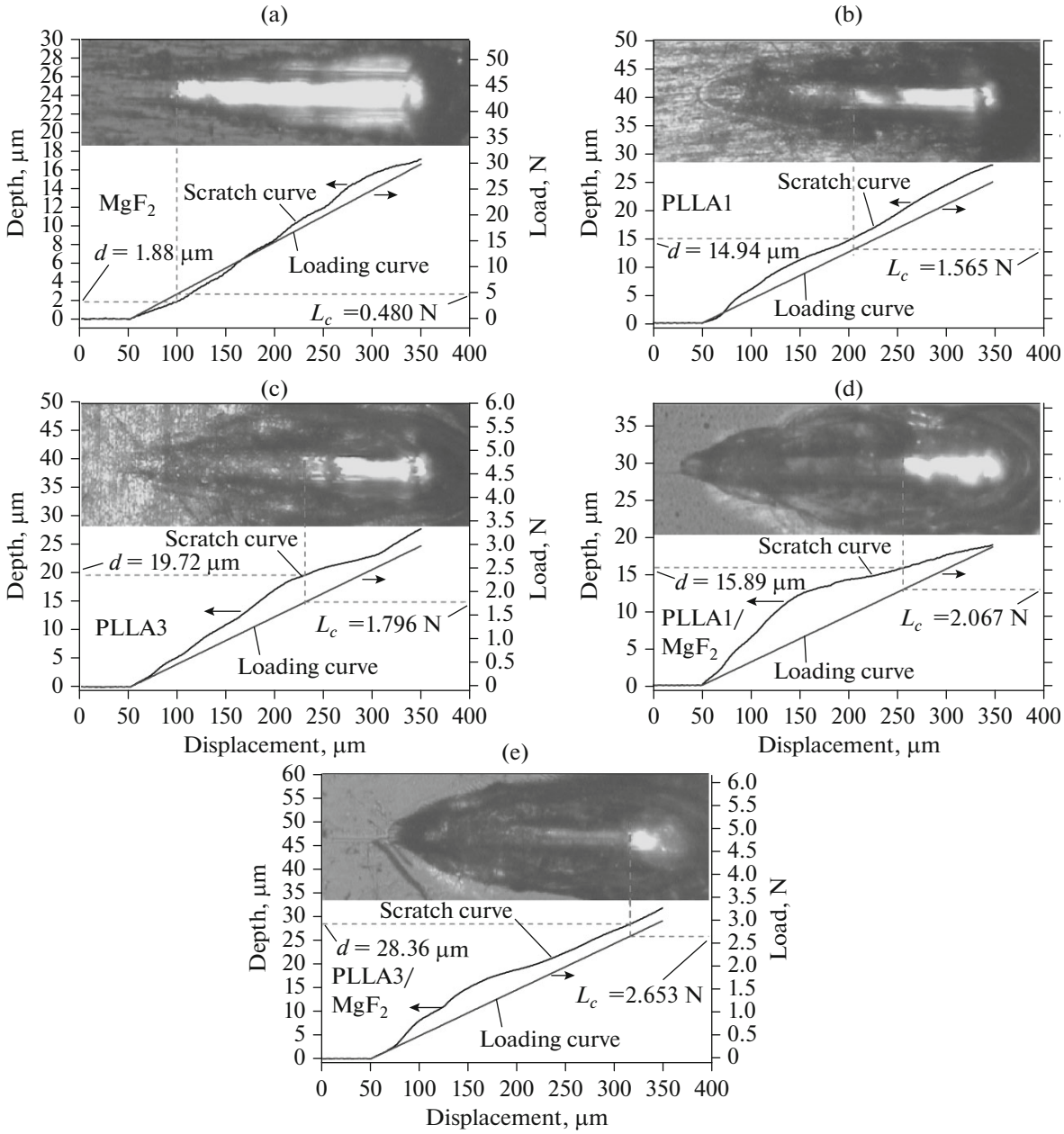

Fig. 4. Schematic illustration of determination on critical load of various coatings on AZ31.

[11]. Additionally, a larger effective contact area of dense PLLA with the substrate than that of the porous MgF_2 may reasonably account for advantageous adhesion of the former over the latter. Alternatively, the composite coating possesses higher adhesion more likely because PLLA solution was infused into the porous MgF_2 layer sealing the pores, healing the flaws and forming a stronger composite bonding layer with organic and inorganic constituents reinforced mutually. Then it can be supposed pinning and interlocking effects caused by PLLA infusion into the porous structure of MgF_2 layer contributes to this reinforcement.

The coating thicknesses detected by means of scratch test, shown in Table 1, are roughly consistent with those observed in SEM images. The thickness of composite coating PLLA1/MgF_2 is smaller than the sum of individual MgF_2 and pure PLLA1 layers, implying a portion of PLLA is accommodated by cellular fluoride layer because of the infiltration of runny PLLA solution under capillary force and centrifugal force during high-speed spinning. On the other hand, subsequent PLLA layers may significantly increase the thickness of the composite coating because of saturation of the MgF_2 layer in addition to rising volume

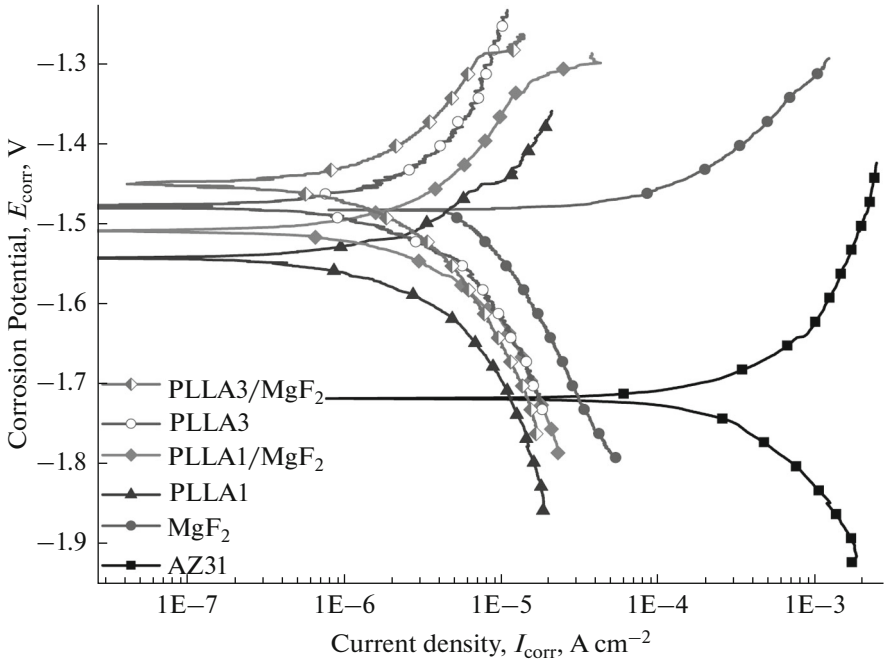

Fig. 5. Polarization curves of bare AZ31 sample and those with various coatings.

of polymer. It is noteworthy that the number of PLLA coating repeats disproportionate the film thickness because multiple spin-coating of PLLA provides partial re-dissolving instead of simple superposition. Apparently, the thickened PLLA layer makes full infusion of fluoride porosity and increases ductility of the whole coating leading to improvement of adhesion.

Corrosion Resistance

Figure 5 depicts the polarization curves of the uncoated AZ31 as well as the coated ones. Three electrochemical parameters i.e. corrosion potentials (E_{corr}), corrosion current density (I_{corr}) and polarization resistance (R_p) derived from these curves and are collected in Table 2. It is well established that materials with more positive E_{corr} has higher chances to resist corrosion, and R_p in parallel to E_{corr} has a strong positive correlation with corrosion resistance, while lower I_{corr} indicates reduced corrosion rate. Comparison of these parameters reveals positive-shifted E_{corr}, rising R_p as well as lowered I_{corr} by two orders of magnitude for the coated AZ31 sample relative to the pristine one suggesting that, overall, the corrosion resistance of magnesium alloy was obviously improved by virtue of coating strategies.

Comparative analysis of the coated counterparts demonstrates that MgF_2 film more effectively raises E_{corr} and PLLA tends more to reduce I_{corr}, and thus a combination of both remarkably improves the capability of simultaneously increasing E_{corr} and decreasing I_{corr}. It seems that the composite coating outperforms either of the solely applied ones with respect to anticorrosion property. Additionally, the PLLA coating allows a more noticeable fall of I_{corr} and rise of R_p than MgF_2 film and multiplying PLLA layers promotes increase in E_{corr}, R_p and decline in I_{corr}. These results prove PLLA is likely to provide a higher corrosion resistance than MgF_2 does. The reason why MgF_2 layer alleviates corrosion to some extent can be ascribed to its insolubility in SBF and labyrinth-like porous structure hindering direct access of corrosive agents, while dense texture and tardy degradation of PLLA may be responsible for its protection against corrosion. A combination of the both will form an

Table 2. Electrochemical parameters of studied coatings and AZ31 magnesium alloy

Sample	AZ31	MgF_2	PLLA1	PLLA1/MgF_2	PLLA3	PLLA3/MgF_2
E_{corr}/V	−1.719	−1.482	−1.544	−1.509	−1.479	−1.450
I_{corr}/A cm^{-2}	2.91×10^{-4}	8.14×10^{-6}	5.09×10^{-6}	6.53×10^{-6}	3.97×10^{-6}	2.93×10^{-6}
R_p/Ω cm^{-2}	51.89	195.94	6701.29	6686.92	8053.58	10618.70

integrated composite system that may further improve the corrosion resistance of magnesium alloy.

CONCLUSIONS

MgF_2 conversion layer formed on AZ31 magnesium alloy by HF treatment with more MgF_2 in the outer layer than in the interface which assumedly composes of MgF_2 and $Mg(OH)_2$. MgF_2 conversion layer possesses a labyrinthine porosity with fine pores interconnected to larger ones, while spin-coated PLLA film is dense and adheres to the substrate seamlessly. PLLA is impregnated into the porous fluoride conversion layer forming an integrated inorganic/organic composite coating. PLLA is more likely to facilitate the improvement in adhesion between the coating and substrate compared to fluoride layer because of its ductility and higher contact area. Infiltration of PLLA into porous MgF_2 layer sealing the pores and flaws contributes to the reinforcement of the composite coating, and thus promotes the improvement of the interfacial adhesion as well as corrosion resistance. The composite coating of PLLA/MgF_2 outperforms either of the solely applied coatings with respect to anticorrosion and adhesion properties under the same condition.

ACKNOWLEDGMENTS

The authors thank the financial support of Natural Science Foundation of Chongqing [grant no. cstc2012jjA50034].

REFERENCES

1. Lu, S.K., Yeh, H.I., Tian, T.Y., and Lee, W.H., Degradation of magnesium alloys in biological solutions and reduced phenotypic expression of endothelial cell grown on these alloys, *IFMBE Proc. Part*, 2007, vol. 5, no. 15, pp. 98–101.
2. Seal, C.K., Vince, K., and Hodgson, M.A., Biodegradable surgical implants based on magnesium alloys—A review of current research, *IOP Conf., Ser.: Mater. Sci. Eng.*, 2009, vol. 4, p. 012011. doi 10.1088/1757-899X/4/1/012011
3. Gu, X.N. and Zheng, Y.F., A review on magnesium alloys as biodegradable materials, *Front. Mater. Sci. China*, 2010, vol. 4, pp. 111–115.
4. Chen, Y., Song, Y., Zhang, S., Li, J., Zhao, C., and Zhang, X., Interaction between a high purity magnesium surface and PCL and PLA coatings during dynamic degradation, *Biomed. Mater.*, 2011, vol. 6, pp. 1–8.
5. Alabbasi, A., Liyanaarachchi, S., and Bobby Kannan, M., Polylactic acid coating on a biodegradable magnesium alloy: An in vitro degradation study by electrochemical impedance spectroscopy, *Thin Solid Films*, 2012, vol. 520, pp. 6841–6844.
6. Yang, J., Cui, F., and Lee, I.S., Surface modifications of magnesium alloys for biomedical applications, *Ann. Biomed. Eng.*, 2011, vol. 39, pp. 1857–1871.
7. Xu, X., Cheng, J., Zhang, C., Yan, X., Zhu, T., Yao, K., Cao, L., and Liu, Y., Bio-corrosion and polymer coating modification of magnesium alloys for medicine, *Rare Met. Mater. Eng.*, 2008, vol. 37, pp. 1225–1228.
8. Mao, L., Yuan, G., Niu, J., Zong, Y., and Ding, W., In vitro degradation behavior and biocompatibility of Mg–Nd–Zn–Zr alloy by hydrofluoric acid treatment, *Mater. Sci. Eng. C*, 2013, vol. 33, pp. 242–250.
9. Jo, J.H., Kang, B.G., Shin, K.S., Kim, H.E., Hahn, B.D., Park, D.S., and Koh, Y.H., Hydroxyapatite coating on magnesium with MgF_2 interlayer for enhanced corrosion resistance and biocompatibility, *J. Mater. Sci: Mater. Med.*, 2011, vol. 22, pp. 2437–2447.
10. Guo, M., Cao, L., Lu, P., Liu, Y., and Xu, X., Anticorrosion and cytocompatibility behavior of MAO/PLLA modified magnesium alloy WE42, *J. Mater. Sci.: Mater. Med.*, 2011, vol. 22, pp. 1735–1740.
11. Shi, P., Niu, B., Chen, Y., and Li, Q., Preparation and characterization of PLA coating and PLA/MAO composite coatings on AZ31 magnesium alloy for improvement of corrosion resistance, *Surf. Coat. Tech.*, 2015, vol. 262, pp. 26–32.
12. Wang, Z.L., Yan, Y.H., Wan, T., and Yang, H., Poly(L-lactic acid)/hydroxyapatite/collagen composite coatings on AZ31 magnesium alloy for biomedical application, *Proc. IMechE, Part H: J. Eng. Med.*, vol. 227, no. 10, pp. 1094–1103.
13. Kokubo, T. and Takadama, H., How useful is SBF in predicting in vivo bone bioactivity?, *Biomaterials*, 2006, vol. 27, pp. 2907–2915.
14. Bakhsheshi-Rad, H.R., Abdul-Kadir, M.R., Idris, M.H., and Farahany, S., Relationship between the corrosion behavior and the thermal characteristics and microstructure of Mg–0.5Ca–*x*Zn alloys, *Corr. Sci.*, 2012, vol. 64, pp. 184–197.
15. Argade, G.R., Kandasamy, K., Panigrahi, S.K., and Mishra, R.S., Corrosion behavior of a friction stir processed rare-earth added magnesium alloy, *Corr. Sci.*, 2012, vol. 58, pp. 321–326.
16. Hou, S.S., Zhang, R.R., Guan, S.K., Ren, C.X., Gao, J.H., Lu, Q.B., and Cui, X.Z., In vitro corrosion behavior of Ti–O film deposited on fluoride-treated Mg–Zn–Y–Nd alloy, *Appl. Surf. Sci.*, 2012, vol. 258, pp. 3571–3577.
17. Bakhsheshi-Rad, H.R., Idris, M.H., and Abdul-Kadir, M.R., Synthesis and in vitro degradation evaluation of the nano-HA/MgF_2 and DCPD/MgF_2 composite coating on biodegradable Mg–Ca–Zn alloy, *Surf. Coat. Tech.*, 2013, vol. 222, pp. 79–89.
18. Yan, T., Tan, L., Xiong, D., Liu, X., Zhang, B., and Yang, K., Fluoride treatment and in vitro corrosion behavior of an AZ31B magnesium alloy, *Mater. Sci. Eng. C*, 2010, vol. 30, pp. 740–748.
19. Wu, L., Dong, J., and Ke, W., Potentiostatic deposition process of fluoride conversion film on AZ31 magnesium alloy in 0.1 M KF solution, *Electrochim. Acta*, 2013, vol. 105, pp. 554–559.
20. Liu, X.K., Liu, Z.L., Liu, P., Xiang, Y.H., Hu, W.B., and Ding, W.J., Properties of fluoride film and its effect on electroless nickel deposition on magnesium alloys, *Trans. Nonferrous Met. Soc. China*, 2010, vol. 20, pp. 2185–2191.